3-DIMENSIONAL FLUID FLOW PROFILE ON A STRUCTURED PDMS SURFACE

Alexander Rockenbach and Uwe Schnakenberg
Institute for Materials in Electrical Engineering, RWTH Aachen University, Aachen, Germany

ABSTRACT

We present a device capable of transporting fluid in an open system along a wall without rotating parts using cilia-like comb rows. For the first time, we show a 3-dimensional image of the flow field along the rows with velocity profiles and mid velocities for all three propagation types obtained in our device, symplectic, antiplectic, and synchronous flow. We show the influence of secondary flow on the device. The methods used allows us to simplify our experiment to just a quarter of data.

INTRODUCTION

The transport of fluids or propelling through fluids is the key ability of creatures living in liquid environments. Several algae, bacteria, and animals are moving themselves with cilia [1]–[5]. Humans are transporting liquids with cilia: Females transport the egg of their ovulation cycle through the fallopian tube [6], or mucus is transported in the human lung though cilia [7]. Ctenophores are jellyfish-like animals which are using conjugated cilia, called comb rows, as propelling mechanism. These animals are in some cases several centimeters in size and are not living in a Stokes flow regime, but using cilia-like structures as propelling mechanism as well [8]–[11].

In microfluidics, the propelling of fluids is easy, but in systems without closed channels propelling is often not easy to implement. Here, the system proposed demonstrates a solution. The transport mechanism of fluid is very similar to the propelling mechanism of Ctenophore, but is still far away from natures perfection [12]–[16]. It is not as efficient as its natural model due to the lower elasticity and the lack of an active mechanism to bend the cilia-like structure, called flap.

The propelling system is made of Polydimethylsiloxane (PDMS) and already described in detail in ref. [17] (Figure 1). The flaps arranged in a comb row of 20 units are 500 µm long and 50 µm thick. With a length of 20 mm they cover the whole device. The flaps are located asymmetrically on 120 µm thick PMDS membranes.

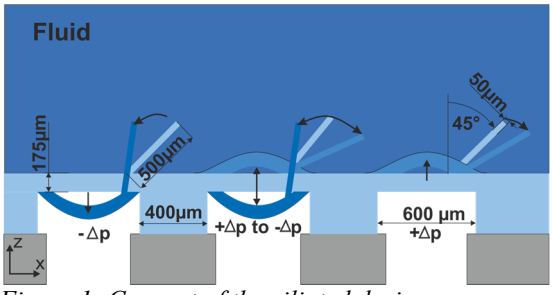

Figure 1: Concept of the ciliated device.

The PDMS device is glued to an adapter. The membranes can be deflected up and down using pneumatic actuation. The asymmetry leads to a deflection of the flap. Overpressure tilts the flap to the right, whereas pressures lower than ambient tilts the flap to the left. In combination with a pre-defined angle between flap and membrane during fabrication this mechanism is able to transport fluids in both directions [18], [19].

METHODS

The fabrication process of the device is described in detail in [18]. Figure 2 shows a close up of the silicone structure. The pneumatic actuation is controlled by a real-time computer (NI cRio 9074, National Instruments Germany GmbH, München, Germany) combined with an amplifier actuating the valves (MHP1-AS-3-M3, Festo, Esslingen, Germany). Finally, the pressure of two reservoirs fed by two pumps is switched by the valves consecutively to the different chambers.

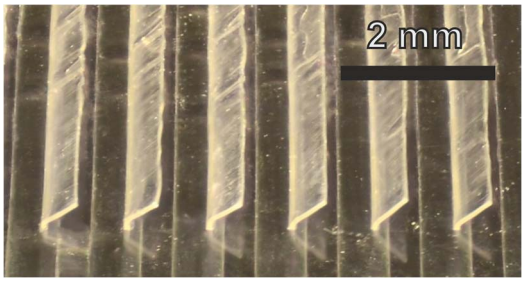

Figure 2: Picture of the realized structure.

Fluid velocity measurements were performed by Particle Image Velocimetry (PIV). A camera (Flea3-U3-13Y3M-C, Point Grey Inc., Canada) was equipped with a telecentric optic of magnification 1. The small depth of field of the objective allows the extraction of small image slices in different depth of the row respective depth of the channel. The used camera is able to generate pictures at defined time points which were applied by a trigger from the valve control unit. All pictures were acquired at the same time of the cycle, so that the flaps are all in the same position.

The positions for taking the pictures were defined by position 1 to 4 shown in Figure 3. For one position, a stroboscopic picture of the surface-near area covering the flaps 1 to 4 were made at first, followed by pictures of area covering flaps 5 to 10, then 11 to 16, and at least 17 to 20, respectively. Position 0 is the beginning of the flaps, whereas position 5 marks the end of the flaps.

Picture post-processing reduces the background by comparing the pictures and deleting fixed pixels. The final pictures shown in Figure 4 are composed by individual pictures. In a last step, the intensity values are scaled as to fit in the 8-bit data format.

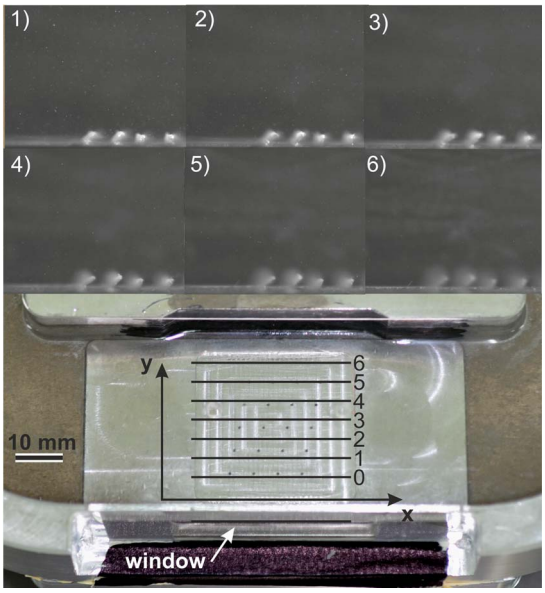

Figure 3: Imaging positions on the ciliated device.

Figure 4 shows those pictures for the four positions along the rows in the flow field. The pictures only show moving particles for the complete time frame, so that one particle in the flow field can be traced for its whole time of emergence in the observed depth of field. White dots in the pictures show particles in one time frame. The same particle in the next time frame is then close to the first and does not have to be divided properly. A distance between images of one particle in two subsequent time points is defined by the distance traveled by the particle in the time between two cycles. Taking this in account the velocity of a particle can be calculated by the length of a cycle and the distance traveled. This calculation was carried out automatically with Trackmate software (Add-on for ImageJ, version 2.7.3, written by Nick Perry, Jean-Yves Tinevez and Johannes Schindelin [20]) and a MATLAB-script. Trackmate generates a list of particle movements in each time frame of an image stack. Then, the script generates velocity profiles shown as a blue plot in each picture in Figure 4.

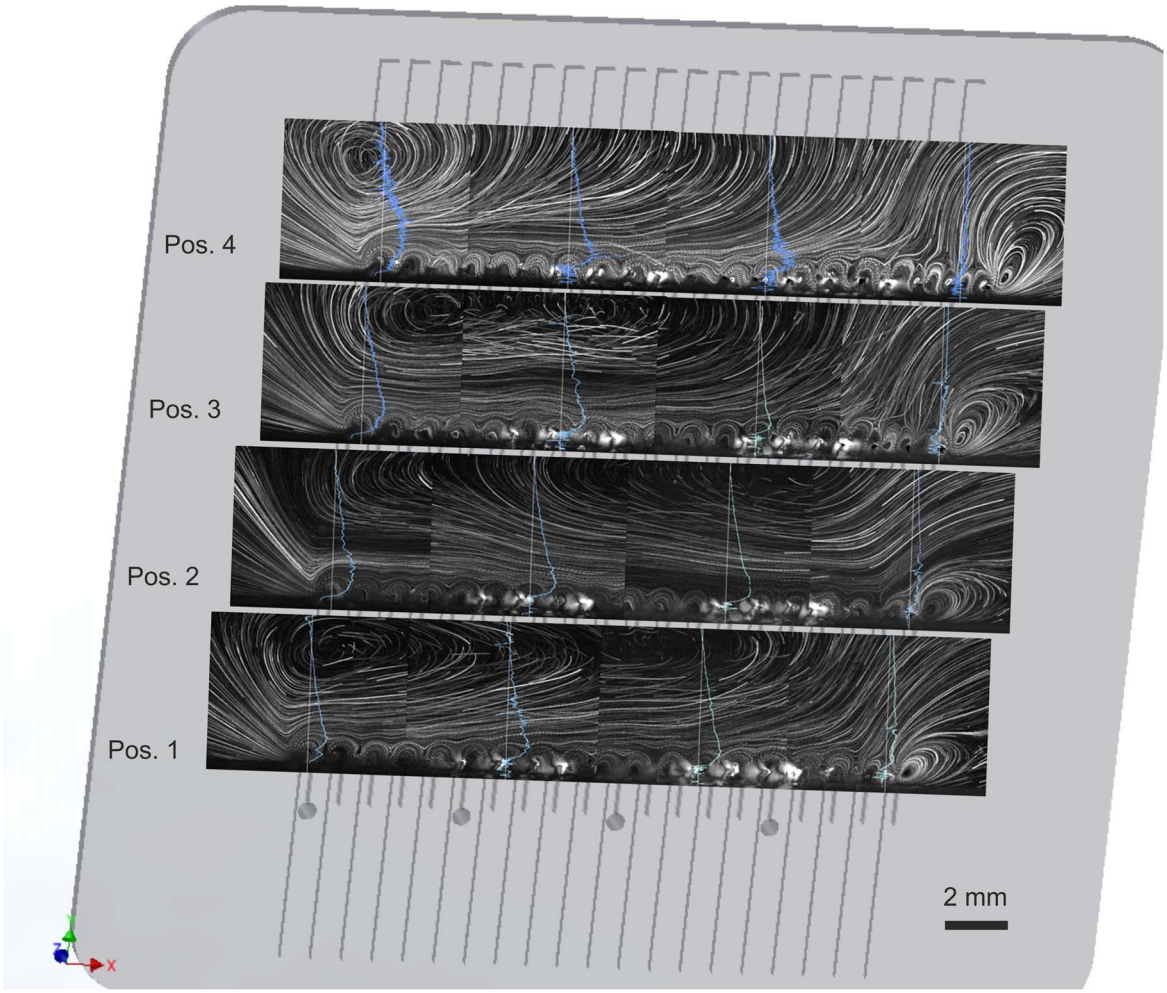

Figure 4: Flow fields along the pneumatically actuated comb row for four positions. A frequency of 7 Hz is applied from left to right. The flaps are tilted by an angle of 30° with respect to plumb line of the membrane. Symplectic fluid propagation is observed.

RESULTS

The overall flow is generated from left to right. Other flow directions than the x-direction were not included in the calculation of the velocity. Movement in negative x-direction is treated as negative velocity. Movements in y-

direction are not included due to the small depth of field.

All calculated velocity profiles show a wall-jet-like profile which is due to the generation of transport at the flap tips [18], [21]. Here, the maximum velocity is generated because the velocity of the flap itself is also at its maximum. Differences from this postulation are caused by fluid flow in other direction as in the x-direction or as failure in the algorithm due to a combination of too high velocities and number of particles in the fluid. In positive z-direction, the velocity decreases slowly until it reduces to zero. In negative z-direction from the tip of the flap the velocity decreases to zero at the wall. Several observed cases do not fit to this postulation, but this is due to the size of the tracer particles in respect to the flow.

Near to the tip of each flap the fluid is flowing in a circular shape due to the impulse of the flap which is tilted by 30°. In experiments not presented here, flaps tilted by 45° are showing a homogeneous flow pattern. Decreasing the angle of the flap leads to a slower velocity and increased circulation. At a distinct flap angle of 20° overall fluid transport is suppressed and only local mixing occurs. Reducing the flap tilting to 0° turns the transport into an antiplectic direction [19].

The complex flow field is unique for the different velocities and propagation types. In Figure 5 the mid velocities of all the 16 stroboscopic pictures are shown for the same device and beating frequency but for different propagation types (A-C). Frequency describes the number of cycles each flap is performing per second and the propagation type is the direction the beating is forwarded from flap to flap in respect to the fluid movement. On the vertical axis the mid velocity of the flow is plotted, whereas the x-axis shows the measurement positions and the y-axis shows the positions from Figure4.

The symplectic flow field in Figure 5A shows negative fluid transport at the right end of the structure at position 2 and 3. Here, the circular flow is very fast and thereby reduces the velocity of the rest of the structure. The circulation in the upper part of the fluid in all positions of Figure 5 has a far lower influence on the total velocity, because of its low velocity. In contrast to symplectic flow antiplectic (Figure 5B) and synchronous (Figure 5C) flow show a flat profile with small differences between the four positions. The velocities of symplectic and antiplectic propagation are around 100µm/s, whereas the synchronous propagation is much lower, around 50 µm/s. This difference is also valid for different frequencies [18].

Figure 5 shows that except the sharp decrease in fluid velocities near the right edges of the comb row in positions 2 and 3 for symplectic flow (see Figure 5A) the differences in fluid velocities are small along the comb row for all three propagation types. The relatively homogeneous velocity profiles give us the possibility to reduce the field of observation to just one position and make qualitative statements for the whole device.

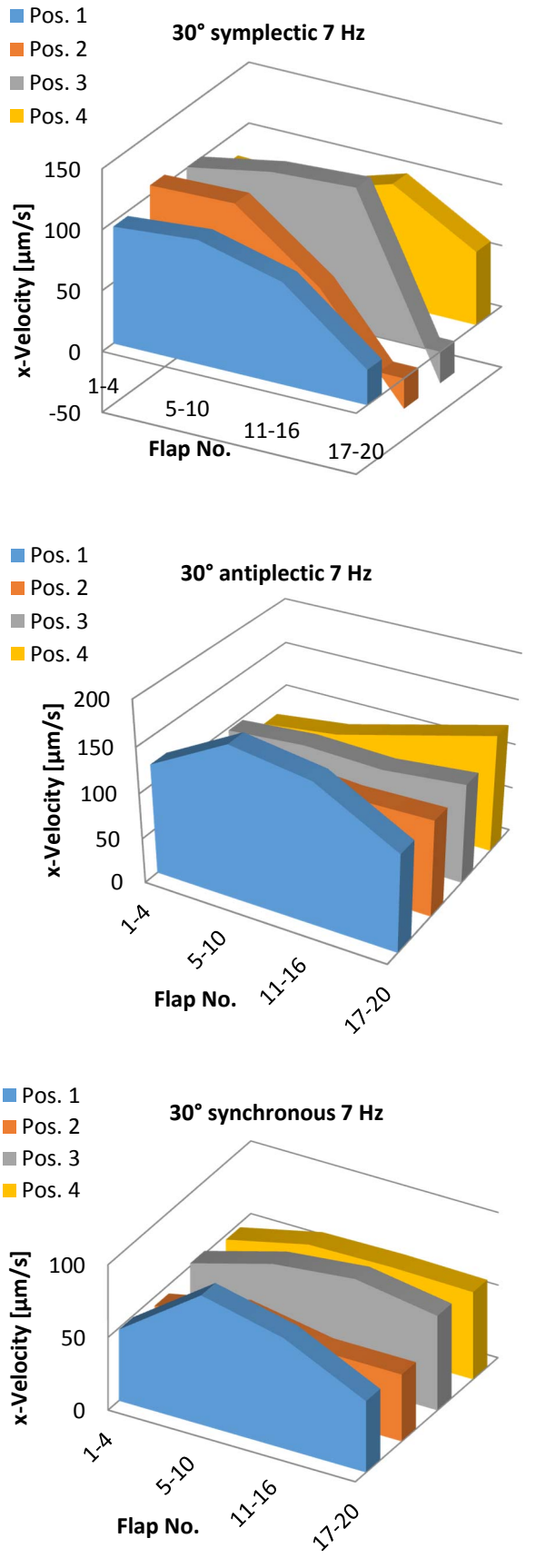

Figure 5: Mid velocities of the flow fields of the different propagation types. The distance from the beginning of the flaps to the position of the measurement is shown in the legend.

In comparison to other studies the data show the fluid flow fields near ciliated walls in large detail [12], [22]–[24] for the first time. Corresponding FEM-FVM (Finite Element Method- Finite Volume Method)- based simulations were carried out and successfully verified by the experimental observations obtained [19]. The beneficial agreement between modeling and experiment offers the opportunity to predict flow profiles and velocities for future device designs and applications. With the here presented 3-dimensional data and the data obtained in simulations the complete flow field can be evaluated from a far lower number of data.

ACKNOWLEDGEMENTS

Funding was granted by the German Federal Ministry of Education and Research under grant 16SV5341 (PaTra) as well as by the German Research Foundation DFG, grant SCHN 587/15-1 within priority program SPP 1726 'Microswimmers'. The authors express their sincere thanks to Professor Dr. Christoph Brücker from City University London, and BAE Systems Sir Richard Olver Chair in Aeronautical Engineering, for his valuable contributions.

REFERENCES

[1] C. Brennen, "Fluid Mechanics of Propulsion by Cilia and Flagella," *Annu. Rev. Fluid Mech.*, vol. 9, pp. 339–398, 1977.

[2] J. R. Davenport and B. K. Yoder, "An incredible decade for the primary cilium: a look at a once-forgotten organelle.," *Am. J. Physiol. Renal Physiol.*, vol. 289, no. 6, pp. F1159–F1169, Dec. 2005.

[3] I. Manton, B. Clarke, and A. D. Greenwood, "Observations with the Electron Microscope on Biciliate and Quadriciliate Zoospores in Green Algae," vol. 6, no. 16, 1954.

[4] K. a. Pitt, C. M. Duarte, C. H. Lucas, K. R. Sutherland, R. H. Condon, H. Mianzan, J. E. Purcell, K. L. Robinson, and S. I. Uye, "Jellyfish Body Plans Provide Allometric Advantages beyond Low Carbon Content," *PLoS One*, vol. 8, no. 8, p. e72683, Jan. 2013.

[5] K. G. Kozminski, K. A. Johnson, P. Forscher, and J. L. Rosenbaum, "A motility in the eukaryotic flagellum unrelated to flagellar beating," vol. 90, no. June, pp. 5519–5523, 1993.

[6] R. a Lyons, E. Saridogan, and O. Djahanbakhch, "The reproductive significance of human Fallopian tube cilia.," *Hum. Reprod. Update*, vol. 12, no. 4, pp. 363–72, 2006.

[7] M. A. Sleigh, J. R. Blake, and N. Llron, "State of Art The Propulsion of Mucus by Cilia," *Am. Rev. Resipratory Dis.*, vol. 137, no. 3, pp. 726–41, 1988.

[8] B. Y. S. L. Tamm, "MECHANICAL SYNCHRONIZATION OF CILIARY BEATING WITHIN COMB PLATES OF CTENOPHORES," vol. 408, pp. 401–408, 1984.

[9] C. L. Craig and A. Okubo, "Physical constrints on the evolution of ctenophore size and shape," *Evol. Ecol.*, vol. 4, no. 2, pp. 115–129, Apr. 1990.

[10] C. L. Craig, A. Okubo, and V. Andreasen, "Effect of spider orb-web and insect oscillations on prey interception," *J. Theor. Biol.*, vol. 115, no. 2, pp. 201–211, 1985.

[11] S. L. Tamm and S. Tamm, "Massive actin bundle couples macrocilia to muscles in the ctenophore Beroë.," *Cell Motil. Cytoskeleton*, vol. 7, no. 2, pp. 116–128, 1987.

[12] B. A. Evans, A. R. Shields, R. L. Carroll, S. Washburn, M. R. Falvo, R. Superfine, C. Hill, N. Carolina, W. Virginia, and V. Uni, "Magnetically Actuated Nanorod Arrays as Biomimetic Cilia," 2007.

[13] B. Evans and R. Superfine, "Design Considerations for Magnetically Actuated Biomimetic Cilia," 2009.

[14] F. Fahrni, M. W. J. Prins, and L. J. van Ijzendoorn, "Micro-fluidic actuation using magnetic artificial cilia.," *Lab Chip*, vol. 9, no. 23, pp. 3413–21, Dec. 2009.

[15] A. R. Shields, B. L. Fiser, B. a Evans, M. R. Falvo, S. Washburn, and R. Superfine, "Biomimetic cilia arrays generate simultaneous pumping and mixing regimes.," *Proc. Natl. Acad. Sci. U. S. A.*, vol. 107, no. 36, pp. 15670–5, Sep. 2010.

[16] E. M. Gauger, M. Downton, and H. Stark, "Fluid transport at low Reynolds number with magnetically actuated artificial cilia," no. 24, pp. 12102–12106, May 2008.

[17] A. Rockenbach, C. Brucker, and U. Schnakenberg, "Pneumatically actuated biomimetic particle transporter," in *Proceedings of the IEEE International Conference on Micro Electro Mechanical Systems (MEMS)*, 2014, pp. 927–930.

[18] A. Rockenbach, V. Mikulich, C. Brücker, and U. Schnakenberg, "Fluid transport via pneumatically actuated waves on a ciliated wall," *J. Micromechanics Microengineering*, vol. 25, no. 12, 2015.

[19] A. Rockenbach and U. Schnakenberg, "The influence of flap inclination angle on fluid transport at ciliated walls," *J. Micromechanics Microengineering*, vol. 27, no. 1, p. 15007, 2017.

[20] J. Schindelin, I. Arganda-Carreras, E. Frise, V. Kaynig, M. Longair, T. Pietzsch, S. Preibisch, C. Rueden, S. Saalfeld, B. Schmid, J.-Y. Tinevez, D. J. White, V. Hartenstein, K. Eliceiri, P. Tomancak, and A. Cardona, "Fiji: an open-source platform for biological-image analysis.," *Nat. Methods*, vol. 9, no. 7, pp. 676–82, Jul. 2012.

[21] D. F. Opaits, M. R. Edwards, S. H. Zaidi, M. N. Shneider, and R. B. Miles, "Surface plasma induced wall jets," no. January, p. 2010, 2010.

[22] B. Pokroy, A. K. Epstein, M. C. M. Persson-Gulda, and J. Aizenberg, "Fabrication of Bioinspired Actuated Nanostructures with Arbitrary Geometry and Stiffness," *Adv. Mater.*, vol. 21, no. 4, pp. 463–469, Jan. 2009.

[23] C. L. van Oosten, C. W. M. Bastiaansen, and D. J. Broer, "Printed artificial cilia from liquid-crystal network actuators modularly driven by light.," *Nat. Mater.*, vol. 8, no. 8, pp. 677–682, Aug. 2009.

[24] L. D. Zarzar, P. Kim, and J. Aizenberg, "Bio-inspired design of submerged hydrogel-actuated polymer microstructures operating in response to pH.," *Adv. Mater.*, vol. 23, no. 12, pp. 1442–6, Mar. 2011.

CONTACT

*U. Schnakenberg, schnakenberg@iwe1.rwth-aachen.de